Experimental analysis and flexural behavior of reinforced-concrete beams reinforced with Glass-fiber-reinforced-polymers

PnD student O. Mariko*,
Department of School of Civil Engineering, the Wuhan University of Technology

1. Introduction

Composite materials made of a cement-based matrix exhibit inherently brittle type failure under tension causes. Brittle failure of cement based composites has been partly alleviated by use of reinforcing steel bars applied in critical regions where tensile stresses arise. Steel is effective however, only after cracking has occurred and the cracked concrete is held together by the reinforcing steel. Design procedures and behavior conventional reinforced concrete are well understood and various design codes and codes of practice all over the world outline steps to achieve a desired design section for any given loading. Building codes have recently imposed stringent seismic design requirements as more knowledge on seismic behavior of structures is available.

The selection of structural materials will sometimes be dictated by variability and/or political and economical constraints. Reinforced concrete is a desirable building material because of one its availability world-wide, two it is relatively cheap and require relatively little energy to produce, and third it does not require very skilled labor to place. In the past two decades there has been rapid growth in application of high strength concrete. High strength concrete have 28-day compressive strengths of 6 000 to 14 000 psi and above (more than two times what was considered normal strength just a few years ago). The high strength permits designers to develop smaller members to carry prescribed loads.

Underdeveloped countries have special problems in selecting building materials in terms of cost, availability of technology. The trend in the developed as well as the under developed countries is to find economically useful applications for readily available raw materials. Natural fibers from plant origins are abundant in most developing countries.

These fibers can be easily and economically extracted. It is appropriate to investigate the feasibility of such fibers in composite building materials.

The art of using fibers to reinforce brittle matrices dates back to the Pharaoh days in Egypt when straw was used in making bricks. Development of composite materials represents a milestone in the history of our civilization. Along with conventional building materials such as steel, concrete, aluminum, and wood, composite materials offer an excellent alternative for a multitude of uses. Concrete is the most widely used construction material, commonly made by mixing Portland cement with sand, crushed rock, and water. Traditionally aggregates have been readily available at economic prices and of qualities to suit all purposes. Concrete satisfies an essential basic property requirement for sustainable building materials, mainly because its production is possible using various secondary raw because its production is possible using various secondary raw materials (wastes for recovery). Besides the reduced extraction of raw materials (especially aggregates) and the conservation of disposal sites, the conservation of non-renewable energy and the emissions connected to it during the production of binding agents (cement) due to the use of secondary raw materials with binding agent properties (such as blast furnace slag, fly ash} can be mentioned. Fiber reinforced polymer (FRP) composites (the combination of two or more materials) have emerged as an evolutionary link in the development of new materials from conventional materials. Used more often in the defense and aerospace industries, advanced composites are beginning to play the role of conventional materials (commodities) used for load-bearing structural components for infrastructure applications. These unique materials are now being used worldwide for building new structures as well as for rehabilitating in-service structures. Application of composites in infrastructural systems on a high-volume basis has come about as a result of the many desirable characteristics of composites that are superior to those of conventional materials such as steel, concrete, and wood.

The fiber architecture or fiber orientation refers to the position of the fiber relative to the axes of the element. Fibers can be oriented along the longitudinal axis of the element (at 0° to the longitudinal axis), transverse to the longitudinal axis (at 90° to the longitudinal axis), or in any other direction at the designer's discretion to achieve optimum product efficiency. This customization flexibility is unique to the fabrication of composites, which gives them versatility in applications. Although fiber orientation in a composite can be so varied that the resulting product is virtually an isotropic material with equal strength in all directions, in most cases composite structural elements are designed with the greatest strength in the direction of the greatest load. For example, for composite reinforcing elements such as bars and tendons, fibers are oriented longitudinally (i.e., in the direction of the applied or anticipated tensile force)

2. Laboratory Testing Procedures

Twelve beams were designed with an adequate amount of longitudinal and shear reinforcement so as to make them fail by crushing of concrete in the central zone. Details of the specimens, materials, test setup and instrumentation are described below.

2.1. Beams Specimens

The experimental program consisted of investigating the effects of varying the reinforcing ratio and the effective depth-to height ratio of six pairs of GFRP RC (reinforced concrete) beams. The total length of each beam was 2050 mm, with a rectangular cross-section B mm wide (variable) and 190 mm deep. The specimens were tested under four-point bending, with 1800 mm total span and 600 mm shear span. The distance between loads was 600 mm (Fig. 1). The shear span was reinforced with sufficient steel stirrups to avoid shear failure (Ø8 mm@70 mm). In the pure bending zone, no stirrups were provided so as not to influence crack development in the constant moment zone. Two 6 mm steel bars were used as top reinforcement to hold stirrups in place in the shear span zone. Three different amounts of longitudinal reinforcement (2Ø12, 2Ø16 and 3Ø16) and two different effective depth-to-height ratios (0.75 and 0.86) were used. The width of the beam was changed to maintain reinforcement ratios of 0.99%, 1.77% and 2.66%, respectively. Two specimens were tested for each type of beam; specimen a was prepared uncracked whilst specimen b had a 3 mm high precrack in the midspan section to ensure the initiation of a crack at this specific position and to facilitate precise measurement of strain in that region.

The pre-crack was created by placing a 1 mm wide steel rectangular section in the moulds prior to casting. The beam specimens are identified as C-wyz-Dx, where wyz stands for the amount of reinforcement (i.e. two diameters of 12 mm is 212) and x stands for the cover of the main rebar (D1 for 20 mm and D2 for 40 mm). Geometric and reinforcement details of the beams are given in Fig. 1 and Table 1.

Table 1. Geometric characteristics of sections

Beam designation	Main Rebar	Width, b (mm)	Cover, c (mm)	d/h	Reinforcement Ratio, ρ (%)
C-212-D1	212	140	20	0.86	0.99
C-216-D1	216	140	20	0.85	1.78
C-316-D1	316	140	20	0.85	2.67
C-212-D2	212	160	40	0.75	0.99
C-216-D2	216	160	40	0.74	1.78
C-316-D2	316	160	40	0.74	2.67

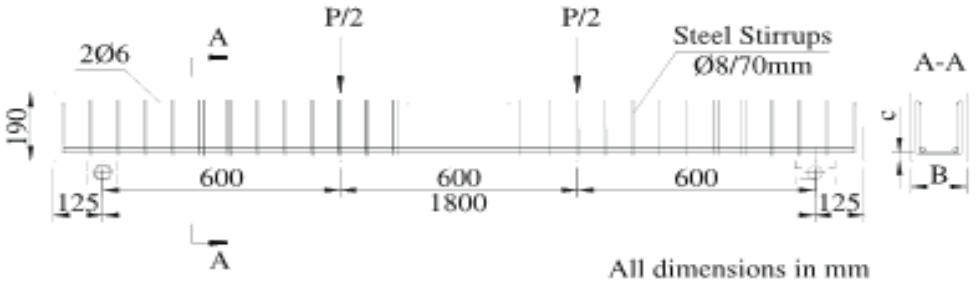

Figure 1. Geometric and reinforcement details

2.1.1. Materials

All beam specimens had a target concrete compressive strength of 50 MPa. Concrete consisted of 162 kg/m^3 of water, 842 kg/m^3 of sand, 940 kg/m^3 of gravel, 385 kg/m^3 of ordinary Portland cement (OPC), a 0.42 water/cement ratio and 0.9% (of the OPC) of superplasticizer. The beams were cast in pairs (specimens a and b) with the same target compressive strength of 50 MPa. The concrete properties were determined from cylinder control samples with a diameter to- height ratio of 1:2 taken directly from the beams after the tests had been performed, due to lack of reliability detected in initial cylinders prepared at the time of the casting. The compressive strength and the modulus of elasticity were tested according to UNE 83.304/84 and ASTM (American Society for Testing and Materilas) C 469/87 standards, respectively. The concrete flexural tensile strength for each pair of beams was calculated from the load-deflection results for the tested beams. The results of the mechanical properties of concrete are summarized in Table 2.

As a flexural reinforcement, ribbed GFRP rebars with 75% of glass content in volume were used. These rebars are manufactured by a pultrusion process, in which boron-free ECR glass fibers are drawn through a tool in a continual process and are impregnated with liquid synthetic vinyl ester-urethane (VEU) resin. The bar is then processed to obtain a ribbed surface (Fig. 2). The tested bars present a relatively high modulus of elasticity (60 GPa, corresponding to the nominal internal diameter) compared to other commonly used GFRP bars (35–45 GPa). Two nominal diameters were used (12 and 16 mm). In Table 3 the mean values of mechanical properties obtained from uniaxial tension tests are shown. The elastic modulus was determined using an external axial extensometer over a

length of 100 mm. This extensometer was removed prior to bar failure to avoid damage, so the strain at failure was not measured.

Table 2 Mechanical properties of concrete

Beam designation	Compressive strength f_c (MPa)	Modulus of Elasticity, Ec (MPa)	Tensile strength, f_{cr} (MPa)
C-212-D1	59.8	26.939	3.5
C-216-D1	56.3	26.524	3.3
C-316-D1	55.2	24.926	3.8
C-212-D2	39.6	23.163	3.0
C-216-D2	61.7	27.318	3.3
C-316-D2	60.1	26.910	3.6

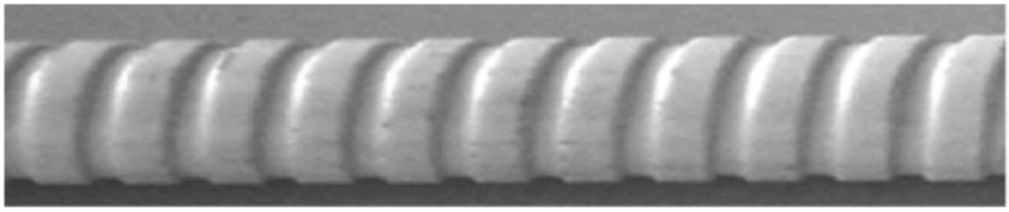

Figure 2. Surface aspect of the GFRP rebars

2.1.2. Experimental setup and instrumentation

A hydraulic jack applied the load to the GFRP RC beam through a spreader beam (Fig. 3). The load was applied in displacement control mode at a displacement rate of 0.8 mm/min and all the data were collected by a data acquisition system. Steps of around 10 kN were applied and after each increment the evolution of cracks and strains was recorded. In order to measure the deflection of the tested beam, three transducers (linear variable differential transformers LVDTs and strain gauge based transducers) were used, one at each support and one in the midspan section. Horizontal top and bottom strains were measured in the midspan zone by means of a mechanical extensometer with a gauge length of 150 mm between Demec points along the central 450 mm of the beam.

Two inclinometers were provided on both sides of the pure bending zone, each one located 225 mm from the midspan section. This configuration allowed sectional rotations to be measured and the average curvature of the pure bending zone to be calculated. An optical magnifier with an accuracy of 0.05 mm was used to measure crack widths. The b beams were additionally instrumented with three concrete strain gauges on the surface of the midspan section (one on the top surface, one 20 mm from the top and one 48 mm from the top) to quantify the evolution of concrete strain with load. Another horizontal transducer was used in the midspan section of these beams at the height of the longitudinal reinforcement to measure the width of the anticipated midspan crack. In addition, the b beams which had 16 mm reinforcement bars (C-216-D1-b, C-216-D2-b, C-316-D1-b, C-316-D2-b) were internally instrumented with strain gauges on the GFRP rebar surface. Four of these gauges were evenly distributed over the shear span length, where as in the midspan zone eight gauges were spaced at 22 mm starting from the midspan section (Fig. 3).

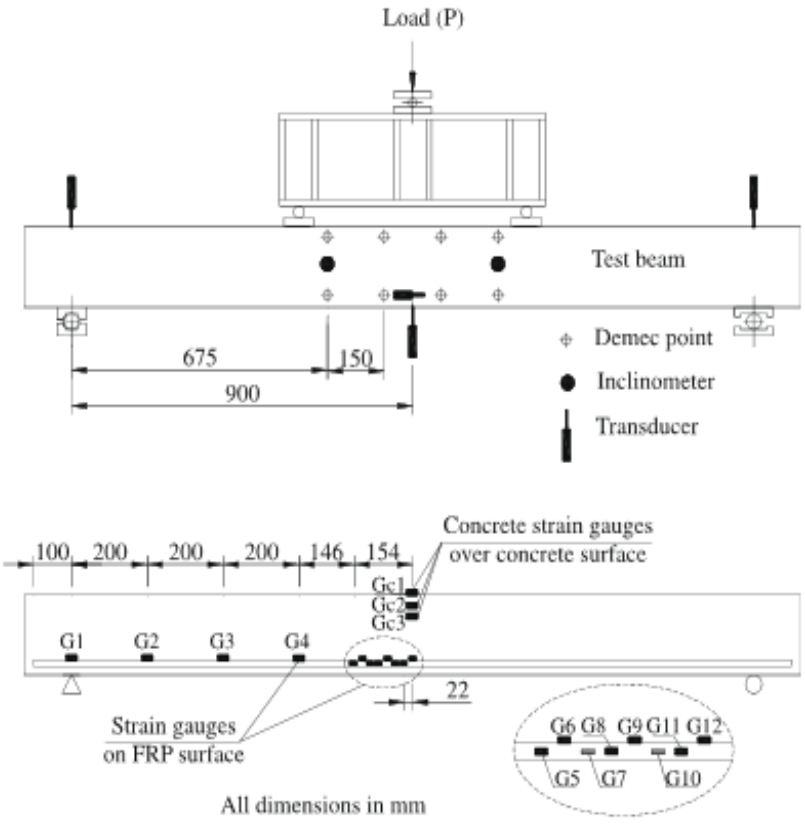

Figure 3. Test setup

2.2. Tensile Test GFRP Rebar

This report summarizes an experimental program that investigated the bond variability of glass-fiber- reinforced-polymer (GFRP) reinforcement in concrete. Tensile tests were also performed on the GFRP rebar for Comparison to bond tests that exhibited bar failure. Eighty-four inverted half-beam bond specimens were tested while monitoring load, loaded-end slip, free-end slip, cracking, and acoustic emissions on the embedded bar and concrete. Three to six replicate tests were conducted for each set of variables. The results of each test within a series were examined to investigate the relative variability with respect to the failure types.

The M1 rebar was observed to rely primarily on mechanical interlock to develop bond strength. This conclusion was based on investigations of the rebar surface condition, bar deformation geometry, slip curves, Acoustic Emission (AE) results, crack patterns and forensic investigations.

Additionally, the ultimate loads for the bond tests with the M1 rebar were affected by changes in embedment lengths but did not vary for tests with 2 and 3*db* cover. The cover may not have had an influence because the majority of the tests failed with ultimate loads within two standard deviations of the tensile test average. A 15.0 in. development length was selected for these bars embedded with 2 or $3d_b$ cover. The corresponding 1/*K1* value for this development length was 15.9.

Overall the M1 rebar had coefficients of variation (COV) of 14.3 and 8.9% for bond tests that exhibited bar failure and tensile test bar failures, respectively. The bond tests that failed in concrete splitting had COVs from 5.2 to 5.9%. The M2 rebar was observed to rely primarily on adhesion and friction to develop bond strength. This conclusion was based on investigations of the rebar surface condition, bar deformation geometry, slip curves, AE results, crack patterns and forensic investigations.

Additionally, the ultimate loads for the bond tests with the M2 rebar were affected by changes in embedment lengths but did not vary for tests with 2 and $3d_b$ cover. A development length was determined by conducting a linear regression through the concrete splitting failures to the tensile test average and reported manufacturer's tensile strength (43.5 kips). The resulting development length was 31.5 in. with a corresponding 1/*K1* value of 17.2. Overall the M2 rebar had a coefficient of variation (COV) of 2.9% for the tensile test bar failures and only one bond test exhibited a bar failure not within the grip. Neither bar was recommended for immediate use as reinforcement in bridge decks. The M1 rebar exhibited cracking and splitting along the outer coating of the bar which damaged bar deformations. Additionally these bars exhibited larger COVs for bar failures with average ultimate loads below the reported manufacturer's value. The M2 rebar exhibited a smaller COV for tensile test bar failures and a similar ultimate load average when compared to the manufacturer's reported strength. However, both GFRP rebar had 47.0 in. embedment length bond tests which exhibited bar failures with ultimate loads less than the tensile test average minus two standard deviations.

2.2.1. Test Procedures

All of the tests were conducted according to the same basic procedure. The concrete specimens were placed into the test frame with the test bar centered on the actuator arm to ensure it was pulled straight. Initially the loaded-end slip linear variable differential transformers (LES LVDTs) brackets were attached directly onto the GFRP rebar with screws tightened onto the bar. After testing a number of M1 specimens, it was apparent the outer coating of the M1 bars was damaged by the screws and the bars would need protection. The initial protection method included application of tape directly to the bar under the screws. Both masking tape and duct tape were used for this protection system. Unfortunately neither tape sufficiently protected the outer coating of the M1 bars. In later tests the bars were wrapped with a nominal 5/8 or 3/4 in. rubber hose, slit for installation and covered with a nominal 1/16 in. thick aluminum strip to distribute the point loads from the screws. after all instrumentation was installed and data acquisition systems activated, the test was run. Each test started with tension load applied through the actuator to the GFRP rebar grip system at 0.05 in./min. This rate was successfully used by Retika in similar tests and was based on ASTM A994, "Comparing Bond Strength of Steel Reinforcing Bars to Concrete Using Beam-End Specimen" and C234, "Comparing Concretes on the Basis of the Bond Developed with Reinforcing Steel." After application of one to two kips of load, the concrete specimen had positioned itself firmly within the load frame and the loading was continued until failure. As surface cracks developed, they were marked with a permanent marker on the specimen which had a pre-drawn grid system. The grid was drawn with a black marker. Each crack and associated load during the test was recorded on the specimen surface with a blue marker. Tests that failed in concrete splitting had additional cracks that occurred at ultimate load. These cracks were recorded on the specimen surface with a red marker.

After failure, the crack pattern was recorded and post test pictures were taken. A careful investigation of the bar and the specimen was done to investigate fiber damage, concrete surface texture and other clues to the debonding process. The testing process culminated with an individual test report that documented the complete test and results.

2.2.2. Pilot Test Parameters

The number of bond tests for the Pilot Study was based on the GFRP rebar available at the time, No. 3 and 5 from M1 and No. 4 and 6 from M2. Tests involving three different embedment lengths for each of the four bar types were initially planned for the Pilot Test. Ideally, the tests at three embedment lengths would provide information regarding the linearity of the GFRP rebar bond relationship with embedment length. In summary, the Pilot Study was to consist of 12 bars, embedded two per half-beam, for a total of six concrete specimens. The three variables for the Pilot Test were the manufacturer, bar size and embedment length. Cover remained constant at 2*db* due to the limited number of tests in the Pilot Study. Additionally, this cover was the most probable and economical cover expected for bridge decks reinforced with GFRP rebar. Manufacturers M1 and M3 were selected for the Pilot Test because they had different deformation systems: Type 1 for the M1 bars and Type 2 for the M2 bars. Both manufacturers supplied two different bar sizes that resulted in four possible test bars: M1-4, M1-5, M2-4 and M2-6. Three lengths were selected for the M1-4 GFRP rebar and four lengths were selected for the M1-5 GFRP rebar. The extra embedment length for the M1-5 GFRP rebar was included because of the lack of comparable test results for bars of this size and deformation type. Two lengths were selected for the M2-4 bars that matched Retika's for direct comparison and three lengths were selected for the M2-6 bars.

The embedment lengths were determined by selecting a desired percentage of the bar's ultimate tensile strength, *fu*, to be achieved in the test. Ideally, this percentage (less than 100%) would result in a concrete splitting failure and not bar fracture. The following percentages were targeted for each GFRP rebar test.

GFRP Rebar Test	% of Bar's Tensile Capacity
GFRP Rebar M1-4	65, 80 and 95%
GFRP Rebar M1-5	65, 75, 85 and 95%
GFRP Rebar M2-4	50 and 65%
GFRP Rebar M2-6	65, 80 and 95%

3. Test Results

3.1. Beams

In this section, the most significant experimental results are presented and compared with predictions obtained from different theoretical approaches. Initially, the midspan section is analyzed, in terms of the strain distribution along the depth of the section and the evolution of neutral axis depth with load. The pure bending zone of the beam is then analyzed, and the moment–curvature relationship examined. Finally, a general analysis of the beam behavior is presented. In this analysis, both ultimate and serviceability limit states are studied by examining GFRP reinforcement strain profile along the beam, load-deflection, cracking behavior, modes of failure, ultimate load and deformability. The calculations for the serviceability state were performed for loads up to 35% of the ultimate load, which is considered to be a value that covers sufficiently the usual range for GFRP RC beams

Using the three strain gauges on the concrete surface of the midspan section, an analysis of strains along the depth of the section is carried out and the experimental neutral axis is deduced. The experimental values are compared with a cracked-section analysis (CSA). CSA is based on a totally cracked section, assumes the Bernoulli hypothesis and does not consider any tension in concrete (Fig. 4). The stress–strain curve adopted for the calculations in the CSA is composed of a parabolic ascending branch and a linear descending branch extended up to the ultimate strain, ε_{cu} (Park and Paulay. In this case, the Eurocode 2 parabolic ascending branch is considered, which allows introduction of the experimental values of the concrete modulus of elasticity E_c, the compressive strength f_c, the strain corresponding to the compressive strength ε_{c0}, and the maximum compressive strain ε_{cu} (Fig. 5).

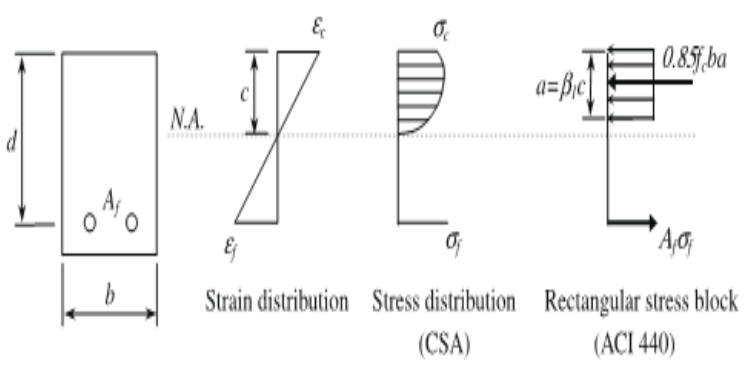

Figure 4. Stress and strain distribution of the cracked-section analysis (CSA) and ACI rectangular stress block

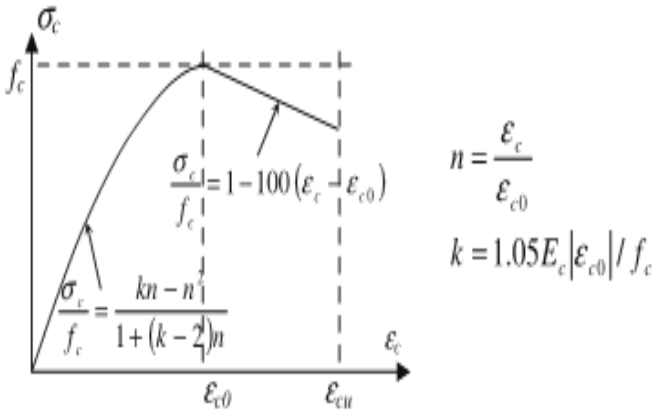

Figure 5. Stress–strain curve adopted for the cracked-section analysis

3.1.1. Strain distribution across the depth of the section

A typical representation of the experimental load-concrete strain relation is shown in Fig. 6a and b. A relatively small first linear branch, corresponding to the uncracked condition, is evident. In this first step of the test, the three experimental curves indicate similar behavior with reduced values of strain. When cracking occurs, the differences among them increase rapidly. As expected, the maximum concrete strain in compression is reached by the top surface strain gauge, while the gauge located 48 mm from the top (Gc3) can be either in compression or in tension, depending on the position of the neutral axis. A higher reinforcement ratio eventually results in a higher depth of the concrete compression block and, therefore, more compressive strain is measured at this last strain gauge.

The experimental strain at the top surface is also compared in Fig. 6a and b with a theoretical prediction of a cracked-section analysis. The CSA fits well with the experimental data. Using the same data, two typical evolutions of the strain profile along the depth of the section for different load levels are represented in Fig. 7a and b. A linear relation between the three strain values is observed, thus confirming the validity of Bernoulli hypothesis, both before and after cracking.

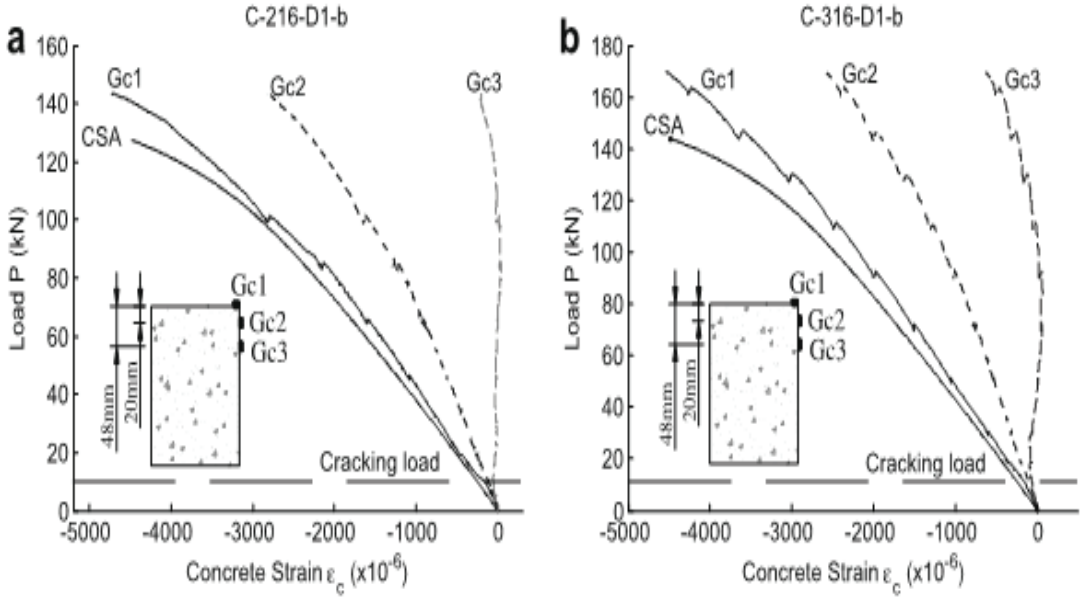

Figure 6. Load-concrete strain (a) Beam C-216-D1-b and (b) Beam C-316-D1-b

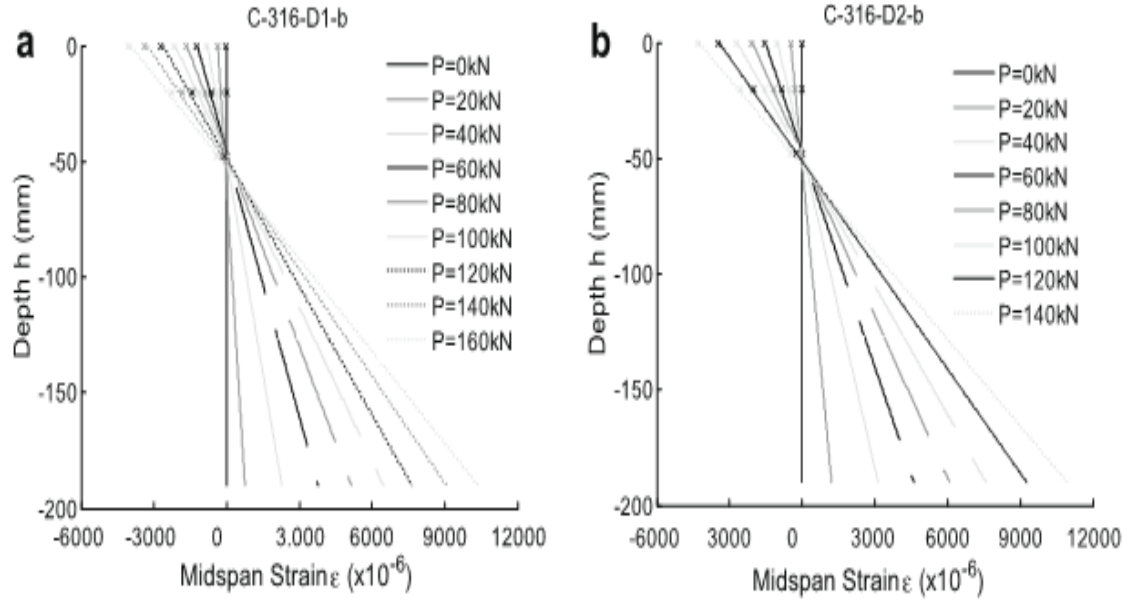

Figure 7. Strain along midspan depth (a) Beam C-316-D1-b and (b) Beam C-316-D2-b

3.1.2. Neutral axis depth

The experimental position of the neutral axis is deduced from the data from the concrete strain gauges. As can be seen in Fig. 8a and b, the neutral axis depth before cracking is located at approximately the mid-height of the section and decreases just after cracking. Then, its value remains constant or decreases slightly, and for high loads it increases until the maximum load is achieved. The neutral axis depth increases with the reinforcement ratio, since equilibrium of forces requires a larger compression block for the greater forces arising from larger areas of reinforcement. The theoretical positions for the neutral axis have been calculated assuming a cracked-section analysis and are shown in Fig. 8a and b. It can be observed that the theoretical prediction compares well with the experimental results

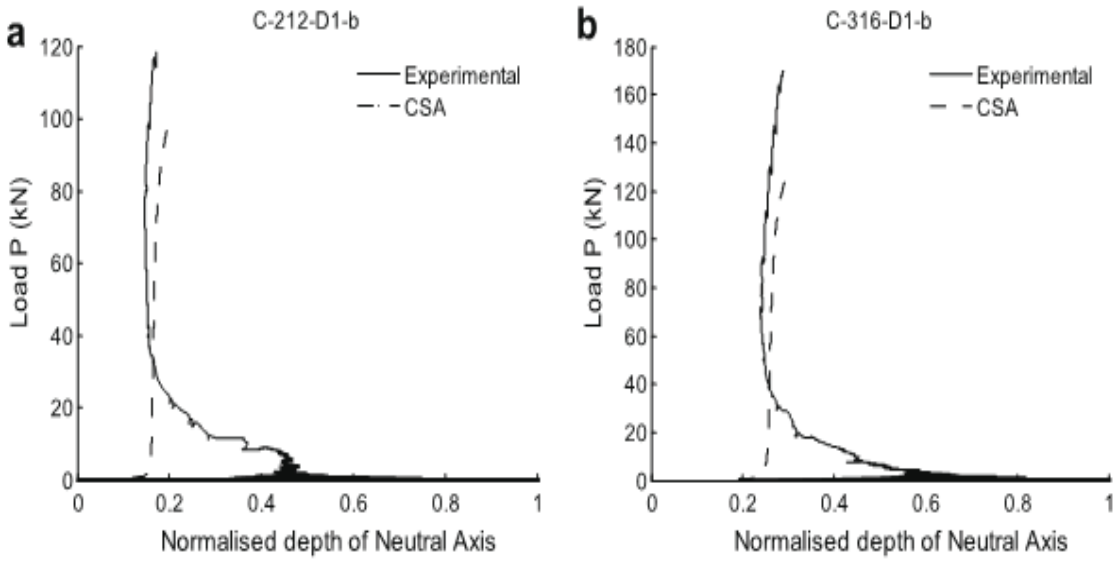

Figure 8. Neutral axis depth (a) Beam C-212-D1-b and (b) Beam C-316-D1-b

3.2. M1 GFRP Rebar

The tests that exhibited bar failures are shown without reference to cover because there was sufficient confinement to contribute to a bar failure regardless of the amount of cover. Each test that failed in concrete splitting is shown with a symbol corresponding to the associated cover.

The variability of the M1 GFRP rebar bond tests was analyzed separately for tests that exhibited bar and concrete failures. Additionally, the hypothesis that increasing embedment lengths should cause an increase in the percentage of tests exhibiting bar failures was examined

The relative induced flexural stress value was not available for test 1M1-5-3-15.0-1 because the LVDTs malfunctioned. Average and standard deviation values of selected tests are given at the bottom of the table. The first values were obtained from using all twenty-five bond tests that exhibited bar failures. The results were further analyzed for factors that would account for the difference and the following criteria were used to eliminate tests from inclusion:

1) type of bar failure observed (specifically bar fracture);
2) bars with damage associated with the LVDT bracket attachment;
3) bars with large amounts of relative induced flexural stress (f_b/σ_{ult}).

The first factor considered was the type of bar failure observed.

Without the rubber/aluminum protection system the outer coatings of the M1 bars were cracked due to the LVDT bracket screws. This cracking reduced the integrity of the bar and probably caused a reduction in the bar tensile capacity. To eliminate this influence, only tests with the rubber/aluminum protection were included in the selected bar failure average.

4. Conclusion

Tests results on 12 GFRP reinforced concrete beams are presented. The reinforcing bars had a relatively high modulus of elasticity and different reinforcement amounts and effective depth-to-height ratios were used. On the basis of the experimental results and prediction models, the following conclusions can be drawn:

All the specimens behaved in a linear way until cracking and, due to lack of plasticity in the reinforcement, almost linearly between cracking and failure, with a greatly reduced slope. However, failure took place at relatively large displacements.

Evaluating the strain values in the midspan section at different load stages showed that Bernoulli hypothesis is valid for both cracked and uncracked sections.

The sectional strains and the neutral axis depth in the midspan section compare well with the numerical predictions based on a cracked-section analysis.

In terms of serviceability behavior, at the service load level the flexural deflection predictions provided by ACI 440.1R-06, Eurocode 2 and Bischoff approaches are in close agreement with the experimental results. However, for higher loads, all these theoretical approaches underestimate deflections, due to the non-linearities that take place at these load levels.

As expected, the parameters chosen in the experimental program (reinforcement ratio and effective depth-to-height ratio) influence the effective stiffness of the beam specimens, and therefore their load-deflection behavior. Nevertheless, all the analytical expressions used to evaluate their response were able to reproduce this variation in the range of serviceability loads reasonably well.

The M1 rebar relied primarily on mechanical interlock to develop bond strength. This bond mechanism for the M1 rebar was postulated by observing the distinct bar deformations which imprinted into the surrounding concrete and lack of concrete particles found adhered to the smooth rebar surface in the forensic investigations. The distinct bar deformations developed bearing on the surrounding concrete that led to a generally linear initial LES curve, lower loads for initial cracking, significant perpendicular cracking and unique AE patterns.

This type of bond development corresponded to an incremental and less uniform bond behavior along the embedment length. It was observed that for these bond tests that the ultimate load for the M1 rebar was affected by embedment length changes but did not significantly vary for tests with 2 and 3*db* cover. The lack of influence from cover was unexpected for the M1 rebar which relied on mechanical interlock for bond strength. However, the majority of the M1 bond tests achieved ultimate loads within two standard deviations of the tensile test average. Hence, these results may not clearly define the effect of cover on ultimate load for the M1 bars. Finally, a development length of 15.0 in. was selected for No. 5 M1 rebar with 2 or 3*db* cover at a concrete compressive strength of 6450 psi. A corresponding 1/*K1* value for the 15.0 in. development length was found to be 15.9.

Bibliography

1. Federation International du Beton, FIB, Task Group 9.3. FRP reinforcement in RC structures, Lausanne, Switzerland; 2007.
2. ISIS Canada. Reinforcing concrete structures with fiber-reinforced polymers – design manual no. 3, Manitoba, Canada: ISIS Canada Corporation; 2001.
3. Benmokrane B, Chaallal O, Masmoudi R. Flexural response of concrete beams reinforced with FRP reinforcing bars. ACI Struct J 1996;91(2):46–55.
4. Masmoudi R, Thériault M, Benmokrane B. Flexural behavior of concrete beams reinforced with deformed fiber reinforced plastic reinforcing rods. ACI Struct J, 1998;95(6):665–76.
5. Brown VL, Bartholomew CL. Long-term deflection of GFRP reinforced concrete beams. In: Fiber Composites in Infrastructure. Proceedings of the 1st international conference on composites in infrastructures (ICCI/96); 1996. p. 389–400.
6. Pecce M, Manfredi G, Cosenza E. Experimental response and code models of GFRP RC beams in bending. J Compos Constr 2000;4(4):182–90.
7. Toutanji HA, Saafi M. Flexural behavior of concrete beams reinforced with glass fiber-reinforced polymer (GFRP) bars. ACI Struct J 2000;97(5):712–9.
8. ACI Committee 318. Building code requirements for structural concrete and commentary (ACI 318-05/ACI 381R-05). Detroit, Michigan (USA): American Concrete Institute; 2005.
9. Faza SS, Ganga Rao HVS. Pre- and post-cracking deflection behaviour of concrete beams reinforced with fiber-reinforced plastic rebars. In: Neale KW, Labossiere P, editors. Proceedings of the first international conference on the use of advanced composite materials in bridges and structures (ACMBSI). Montreal: Canadian Society for Civil Engineering; 1992. p. 151–60.

** Ousmane Mariko, Wuhan, Hubei, China*
Tel. mob.: +86-158-72-39-74-34; e-mail: ousmanemarik@yahoo.fr